

**NASA TECHNICAL
MEMORANDUM**



NASA TM X-3207

NASA TM X-3207

(NASA-TM-X-3207) FLIGHT INVESTIGATION OF
INSTALLATION EFFECTS ON A WEDGE NOZZLE
INSTALLED ON AN UNDERWING NACELLE (NASA)
40 p HC \$3.75

CSCL 21E

N75-21282

Unclass

H1/07 19072

**FLIGHT INVESTIGATION OF INSTALLATION
EFFECTS ON A WEDGE NOZZLE INSTALLED
ON AN UNDERWING NACELLE**

Albert L. Johns

Lewis Research Center

Cleveland, Ohio 44135



1. Report No. NASA TM X -3207	2. Government Accession No.	3. Recipient's Catalog No.	
4. Title and Subtitle FLIGHT INVESTIGATION OF INSTALLATION EFFECTS ON A WEDGE NOZZLE INSTALLED ON AN UNDERWING NACELLE		5. Report Date April 1975	
		6. Performing Organization Code	
7. Author(s) Albert L. Johns		8. Performing Organization Report No. E-8100	
		10. Work Unit No. 505-04	
9. Performing Organization Name and Address Lewis Research Center National Aeronautics and Space Administration Cleveland, Ohio 44135		11. Contract or Grant No.	
		13. Type of Report and Period Covered Technical Memorandum	
12. Sponsoring Agency Name and Address National Aeronautics and Space Administration Washington, D.C. 20546		14. Sponsoring Agency Code	
15. Supplementary Notes			
16. Abstract <p>A flight research program was conducted using a modified F-106B aircraft with an underwing-nacelle - engine installation to investigate installation effects on a wedge nozzle with retracted shrouds from Mach 0.70 to 1.10. These configurations simulated the subsonic flight geometries of a variable-geometry wedge nozzle design for Mach 2.70 operation. The nozzle was tested with a J85-GE-13 turbojet engine, and data were compared with that of 0.34-scale isolated wind tunnel model. Data are also compared with the flight results of a boattail plug nozzle and a cylindrical nacelle plug nozzle. A favorable installation effect occurred from Mach 0.82 to 0.96 with a nominal 4-percent corrected secondary weight-flow ratio. This favorable effect resulted from changes in pressure forces on the nozzle surfaces. The wedge nozzle gross thrust coefficient was about the same as the boattail nacelle plug nozzle and 2.50 to 1.30 percent higher than the cylindrical nacelle plug nozzle over the subsonic Mach number range.</p>			
17. Key Words (Suggested by Author(s)) Airframe installation effects; Propulsion system; Wedge nozzle; Nozzle; Flight test; Underwing nacelles		18. Distribution Statement Unclassified - unlimited STAR category 07 (rev.)	
19. Security Classif. (of this report) Unclassified	20. Security Classif. (of this page) Unclassified	21. No. of Pages 39	22. Price* \$3.75

* For sale by the National Technical Information Service, Springfield, Virginia 22151

CONTENTS

	Page
SUMMARY	1
INTRODUCTION	2
SYMBOLS	3
APPARATUS AND PROCEDURE.	4
Installation	4
Test Configurations	5
INSTRUMENTATION	6
PROCEDURE	6
DATA REDUCTION	7
RESULTS AND DISCUSSION	7
Installation Effects	7
Comparison of the Wedge and Plug Nozzles Performance	8
Comparison of Installed Nozzle Performance Characteristics With and Without Sideplates	9
Effect of Secondary Flow on Installed Wedge Nozzle Configurations Performance Characteristics	10
Pressure Distributions	10
Comparisons of Secondary Flow Effect on Wedge and Plug Nozzle Performance Characteristics	12
SUMMARY OF RESULTS	13
REFERENCES	14

FLIGHT INVESTIGATION OF INSTALLATION EFFECTS ON A WEDGE NOZZLE INSTALLED ON AN UNDERWING NACELLE

by Albert L. Johns

Lewis Research Center

SUMMARY

A flight research program was conducted using a modified F-106B aircraft with an underwing-nacelle - engine installation to investigate installation effects on a wedge nozzle with retracted shrouds from Mach number of 0.70 to 1.10. Installation effects were determined by comparing the in-flight performance with 0.34-scale isolated cold-flow results obtained in the Lewis 8- by 6-foot supersonic wind tunnel. The configurations tested simulate subsonic geometries of a nozzle designed for high nozzle-pressure-ratio operation. In addition to Mach number, variables included a retracted shroud with and without sideplates, corrected secondary flow ratio, and nozzle pressure ratio.

A favorable installation effect occurred from approximately Mach 0.82 to 0.96 with a nominal 4-percent corrected secondary weight-flow ratio. A maximum difference of 5.3 percentage points in gross thrust coefficient occurred at Mach 0.95 (0.966 and 0.913 for the installed and isolated wedge nozzles, respectively). From Mach 0.97 to 1.00 there was an adverse installation effect caused by the terminal shock moving off the nozzle with resulting low static pressures. The favorable installation effect was a result of the pressure rise behind the terminal shock due to the interaction of the wing and nacelle flow fields. This pressure rise causes the pressure forces on the installed wedge nozzle to be higher than those on the isolated wedge nozzle.

Comparison of installed flight performance between the wedge nozzle (retracted shroud without sideplates) and a boattail nacelle plug nozzle (the best inflight plug nozzle tested) indicates both performed at about the same level, over the subsonic Mach number range at military power, and at a corrected secondary weight flow of 4 percent. However, the wedge nozzle subsonic performance was substantially higher than that of a cylindrical nacelle plug nozzle, which has a similar design concept to that of the wedge nozzle.

INTRODUCTION

As part of a program in airbreathing propulsion, Lewis is investigating airframe installation effects on the performance of various exhaust-nozzle concepts appropriate for supersonic-cruise aircraft. The local flow field in the vicinity of an installed nozzle may vary from isolated tests conditions, thereby affecting nozzle performance characteristics (ref. 1). One of the more desirable locations for the propulsion system of aircraft that must cruise efficiently at both subsonic and supersonic speeds is in aft-mounted underwing nacelles. In this location the nacelle inlet is shielded by the wing lower surface to minimize the effects of angle-of-attack. Other favorable interference effects between the nacelle and wing flow fields may minimize drag at important flight conditions (ref. 2).

Flight tests have been made for several exhaust-nozzle concepts which included: an auxiliary-inlet ejector, variable flap ejectors, and low-angle plug nozzles. The performance of these nozzles are reported in references 3 to 5. These tests have shown both favorable and unfavorable installation effects.

Another nozzle concept of interest is a wedge nozzle (refs. 6 and 7). This concept is similar to that of the plug nozzle but utilizes a two-dimensional wedge surface rather than a conical plug. As with the plug nozzle, a cylindrical outer shroud is translated to regulate the internal expansion as nozzle-pressure ratio increases.

The wedge nozzle concept may provide alternative solutions to the mechanical and cooling problems of the axisymmetric plug. For example, the mechanics of achieving a variable-area throat may be simplified by moving a portion of the wedge surface. Accessibility for secondary cooling air is also improved by ducting air through openings along the sides of the wedge for cooling the wedge surface and actuator mechanisms. Also, the wedge nozzle concept can provide an alternative solution to the base drag problem that is associated with twin-engine-fuselage and twin-engine-pod installations. For instance, a wedge could be used as the expansion surface for a twin-engine installation thus eliminating or reducing the base region created by axisymmetric twin nozzles. Also, some modifications to the present wedge could make it suitable for an over-the-wing concept that could have a lower noise level. In addition to this noise advantage, there could be one just because of directivity effects with the wedge installed under-the-wing horizontally.

This report presents the installed performance of the wedge nozzle and a com-

parison with isolated cold-flow model results obtained at Lewis (ref. 6). The present test installation consisted of a podded engine mounted near the aft lower surface of the wing with the wedge nozzle extending beyond the wing trailing edge. These tests were conducted with an F-106B aircraft modified to carry two 63.5-centimeter (25.0-in.) diameter nacelles. The nozzle was installed in the right nacelle and had a 10° half-angle wedge with a fixed primary throat area 729 square centimeters (113 in.^2). This configuration permitted operation at part speed and at military power. The primary jet exhaust was provided by a calibrated turbojet engine (J85-GE-13); the secondary air was obtained from the nacelle inlet. The engine was operated over a range of power settings that resulted in primary exhaust temperature variation from 817.3 to 974.9 K (1471.22° to 1754.94° R). Corrected secondary weight flow ratio varied from 0.0343 to 0.0871. The nozzle was flight tested from Mach 0.70 to 1.10 and from an altitude variation of 4544 to 7650 meters (14 907 to 25 099 ft).

SYMBOLS

A_e	effective area, cm^2 (in.^2)
C_p	pressure coefficient, $(p - p_0)/q_0$
D	nozzle drag, N (lb)
F	nozzle gross thrust, N (lb)
$(F - D)/F_{ip}$	nozzle gross thrust coefficient
h	pressure altitude, m (ft)
l	wedge length measured from primary
l'	boattail nacelle plug length, 92.46 cm (36.40 in.)
l''	cylindrical nacelle plug length, 123.04 cm (48.44 in.) nozzle exit (nacelle station at 549.33 cm (216.27 in.)) to wedge tip (nacelle station 636.09 cm (250.43 in.)), = 86.77 cm (34.16 in.)
M_0	flight Mach number
m	inlet capture mass flow, kg/sec (lb/sec)

P	total pressure, kN/m^2 (psia)
P_8/P_0	nozzle pressure ratio
p	static pressure, kN/m^2 (psia)
q	dynamic pressure, $0.7 p_0 \cdot M^2$, kN/m^2 (psi)
T	total temperature, K ($^{\circ}\text{R}$)
V	velocity, m/sec (ft/sec)
W	weight flow, kg/sec (lb/sec)
x	axial distance measured from primary nozzle exit, nacelle station 549.30 cm (216.27 in.)
x'	axial distance measured from estimated primary throat of boattail nacelle plug nozzle, -15.81 cm (-6.22 in.)
x''	axial distance measured from estimated primary throat of cylindrical nacelle plug nozzle, -14.76 (-5.81)
α_o	angle of attack, deg
γ_e	angle of elevon deflection, deg
$\omega\sqrt{\tau}$	corrected secondary weight flow ratio, $(W_s/W_8)\sqrt{T_s/T_8}$

Subscripts:

ip	one-dimensional isentropic expansion of primary flow
s	secondary
x	condition at axial distance x
0	free stream
8	nozzle throat

APPARATUS AND PROCEDURE

Installation

This research program was conducted with an F-106B aircraft modified to carry two underwing nacelles. The F-106B is shown in figure 1 with a previously tested

plug nozzle (ref. 5) and with a reference nozzle used to calibrate the nacelle drag force (ref. 8). A schematic view of the test installation is shown in figure 2. The 63.5-centimeter (25.0-in.) diameter nacelles were located at approximately 32 per cent semispan with the exhaust nozzle extending beyond the wing trailing edge. Since the nozzle would interfere with normal elevon movement, the section of the elevon directly over the nozzle was rigidly fixed to the wing.

The nacelle had a normal shock inlet and contained a calibrated J85-GE-13 afterburning turbojet engine. Secondary air to cool the engine and afterburner can was supplied from the inlet and was controlled at the periphery of the compressor face by a calibrated rotary valve. The inlet faired into a bulged section on the bottom of the nacelle to accommodate the engine accessory package.

The nacelle was attached to the wing by two links normal to the nacelle axis, and the axial force was measured by a load cell attached to the wing (fig. 2). An accelerometer in the nacelle allowed the load cell to be compensated for axial acceleration. The axial force transmitted to the compensated load cell can be divided into two parts: (1) nacelle drag forward of the research nozzle, referred to as the tare force and (2) research-nozzle gross thrust minus drag. From a Mach number of 0.80 the tare force was determined from research test data that were obtained by using a calibrated cylindrical ejector nozzle (ref. 8). Tare force at a flight Mach number of 0.70 was calculated to be the sum of the ram drag plus the skin friction drag on the nacelle and strut as was used in reference 9 at a Mach number of 0.40. The research-nozzle gross thrust minus the drag was determined by adding the tare force from the compensated load-cell measurements.

Test Configurations

Several views of the wedge nozzle with the retracted shroud without sideplates are shown in figure 3. Figure 4 shows the same views for the retracted shroud with sideplates. The test configurations consisted of a 10° half-angle-wedge centerbody attached to an afterburner can (fig. 5(a)). Coordinates for the contour of the forward portion of the wedge are given in table I. A secondary flow passage is provided between the primary nozzle and the shroud for cooling the afterburner can and primary nozzle. Cutouts in the sides of the wedge provided access for secondary flow for wedge cooling air or for base bleed with truncated wedge configurations.

The nozzle throat was fixed at 729 cm^2 (113 in.^2). The maximum primary flap angle of 10° occurred only at the plan view centerline (top and bottom of fig. 5(a)) and washed out to 0° at the sides of the wedge. (See top view of fig. 5(a).) Dimensional details of the primary nozzle and of the retracted shroud without sideplates are also shown in figure 5(a). Details of the retracted shroud with sideplates are shown in figure 5(b). The sideplates were swept at $25^\circ 30'$. The sideplates were designed such that at supersonic cruise the tip of the sideplates coincided with the tip of the wedge, and the initial Mach line from the top and bottom intercepted the wedge tip. Both shroud configurations had a 10° boattail angle.

INSTRUMENTATION

Secondary total pressures and temperatures were measured with pitot probes and thermocouples, respectively (fig. 6). The probes were located at 0° , 90° , 180° , and 270° . The thermocouples were Chromel/Alumel and had radiation shields. Instrumentation for the external shrouds and primary nozzle are shown in figure 7(a). The external shroud pressure orifices were located circumferentially at $x/l = -0.297$ without sideplates and $x/l = -0.268$ with sideplates. The primary flap pressure orifices were located at 0° . Static-pressure orifices were located on both sides of the wedge (fig. 7(b)).

An onboard digital data system was used to record the pressures and temperatures on magnetic tape (ref. 8). It has the capability of recording 578 parameters in 11.6 seconds.

A flight-calibrated test boom located on the aircraft nose was used to determine free-stream static and total pressures, aircraft angle of attack, and yaw angle.

PROCEDURE

Performance characteristics of the wedge nozzle were obtained over a flight Mach number range from 0.7 to 1.10 and at Reynolds numbers from 10.29×10^6 per centimeter (3.14×10^6 /ft) at Mach 0.7 to 12.16×10^6 per centimeter (3.71×10^6 /ft) at Mach 1.10. The aircraft was flown at the nominal altitude Mach number profile shown in figure 8, which resulted in the angles of attack and elevon deflection shown in figure 9. The nozzle-pressure ratio schedule is given in figure 10 as a function of Mach number. Data were taken at military power settings and part

power at selected Mach numbers. Corrected-secondary-weight-flow ratio $\omega\sqrt{\tau}$ was varied from 0.0343 to 0.0871.

DATA REDUCTION

Engine airflow was determined using prior engine calibration data (ref. 10) along with in-flight measurements of engine speed, pressure, and temperature at the compressor face. Knowing compressor inlet flow, the total pressure and temperature at the turbine discharge, and the fuel flow rates, other parameters at the primary nozzle exit, such as effective area $A_{e,8}$, total pressure P_8 , and total temperature T_8 were obtained from previous calibrations. Calibrations of the secondary-flow-valve pressure drop and position were used to determine the secondary airflow.

The basic nozzle performance parameter presented is the nozzle gross-thrust coefficient which is the ratio of actual gross thrust minus drag to the ideal thrust of the primary flow. The ideal thrust of the primary was calculated from the known mass-flow rate. The mass-flow ratio is expanded isentropically from its value of total pressure and temperature to ambient pressure. Individual pressure distributions are shown for various component surfaces.

RESULTS AND DISCUSSION

Installation Effects

To investigate the effect of installation on the wedge nozzle performance, flight results for a takeoff configuration (retracted shroud without sideplates) were compared with results of a 21.6-centimeter (8.5-in.) wedge nozzle tested in the 8- by 6-foot supersonic wind tunnel (ref. 6). This model is a 0.34-scale of the present flight configuration, but it differed from the flight model in that the forward portion of the wedge, upstream of the nozzle throat, had a shorter leading edge to the nozzle throat. The longer leading edge to the nozzle throat was added to reduce the sonic line distortion at the throat, hence, improving the performance at the higher nozzle-pressure ratios (supersonic cruise). But at the low pressure ratios (subsonic conditions) results from reference 6 show that the longer leading edge to the throat had no significant effect on the nozzle performance.

The installation effect on nozzle gross thrust coefficient and secondary flow

pumping characteristics is shown in figure 11 over the flight Mach number range at a nominal corrected secondary weight flow ratio of 4 percent. A favorable installation effect occurred from Mach 0.82 to 0.96. This favorable effect was the result of the nacelle being located in a favorable wing flow field, which caused a high-pressure region on the nozzle assembly. Because of the small area of the primary nozzle and shroud boattails, most of the favorable effect was produced by pressure acting on the wedge surface. Above Mach 0.95 performance dropped sharply, and at Mach 0.965 nozzle performance became less than that of the isolated wedge nozzle. This drop in performance is a result of the terminal shock moving off the installed nozzle assembly and causing a low static-pressure field. The data of reference 11 show that, because of the wind-tunnel interference, the terminal shock moves off the isolated strut supported jet-exit model at about Mach 1.10.

There was no significant installation effect on the secondary-flow pumping characteristics (fig. 11). Also shown in this figure is the curve of p_0/P_8 . As expected, there was no pumping with a fully retracted shroud.

Installation effect on nozzle performance characteristics at Mach 0.90 is shown in figure 12 for 4-percent corrected secondary weight flow ratio over a nozzle pressure ratio range. At this Mach number (0.90) the installed nozzle is in a favorable flow field; therefore, the gross thrust coefficient is higher than the isolated wedge nozzle. Although there are a limited amount of flight data, it appears that the trend is the same as the isolated nozzle (ref. 6); that is, the gross thrust coefficient was insensitive to nozzle pressure ratio. Also shown in figure 12 is the secondary-flow pumping characteristics and a reference curve of p_0/P_8 . The trend was the same for both the installed and isolated wedge nozzles. There was no significant installation effect over the nozzle-pressure ratio range. In addition, there was no pumping with either model.

Comparison of the Wedge and Plug Nozzles Performance

The two types of plug nozzles selected for comparison are

- (1) The boattail nacelle plug nozzle which had a 14° trailing-edge angle with a rounded primary flap. The primary nozzle simulated a hinged iris primary. The efficiency of this plug nozzle depends to a large degree on the pressure force on the external surface of the primary flap. This nozzle had the best nozzle gross-thrust coefficient of any inflight plug nozzle tested (refs. 5 and 12).

(2) The cylindrical nacelle plug nozzle had a 17° half-angle conical primary flap and represented a hinge-iris-type primary nozzle operating at its minimum area with a capability of 60-percent area modulation. This plug nozzle is similar to the wedge nozzle in that it had large centerbody-to-nacelle area ratio.

Table II shows the nozzle projected area ratios for the wedge nozzle and for both the boattail and cylindrical nacelle plug nozzles.

A comparison of the wedge nozzle with the plug nozzles at military power setting and a nominal corrected secondary weight flow ratio of 4 percent is shown in figure 13 over the flight Mach number range. The nozzle gross-thrust coefficient for both the wedge and the boattail nacelle plug nozzle were about the same. However, the cylindrical nacelle plug nozzle was 2.5-percent lower in nozzle gross thrust coefficient.

Comparison of Installed Nozzle Performance Characteristics

With and Without Sideplates

A comparison of the wedge nozzle performance characteristics with and without sideplates is presented in figures 14 to 22. The effect of Mach number on the gross thrust coefficient and pumping characteristics is shown in figure 14 for 4- and 8-percent corrected secondary flow at military power setting. The retracted shroud without sideplates was about 1 percent higher in gross thrust coefficient with 4-percent corrected secondary flow (fig. 14(a)). For example, at $M_0 = 0.90$ the nozzle gross thrust coefficient was 0.956 and 0.947 with and without sideplates, respectively. This difference in gross thrust coefficient occurred from Mach 0.80 to 0.90. These differences were caused by the increased friction drag on the external shroud and the increase in boattail drag due to the external shape of the sideplate configuration. There was very little difference in secondary-flow pumping characteristics over the Mach number range. With 8-percent secondary flow (fig. 14(b)), the retracted shroud without sideplates had only a slightly higher performance up to Mach 0.94. The pumping characteristics were the same for both configurations.

A comparison of the effect of nozzle-pressure ratio on gross thrust coefficient with and without sideplates is shown in figure 15 for corrected secondary weight flow ratios of 4 and 8 percent at a flight Mach number of 0.90. As indicated in the previous figure and as shown in figure 15(a), at $\omega\sqrt{\tau} = 0.04$ the most desirable

configuration at $M_0 = 0.90$ is the retracted shroud without sideplates. With 8-percent corrected secondary weight flow (fig. 15(b)), the nozzle performance for both configurations was approximately the same over the nozzle pressure ratio range.

Effect of Secondary Flow on Installed Wedge Nozzle Configurations

Performance Characteristics

The effect of corrected secondary weight flow ratio on nozzle gross thrust coefficient for various flight Mach numbers and nozzle pressure ratios is shown in figure 16. Data for the retracted shroud without sideplates are presented in figure 16(a) and with sideplates in figure 16(b). The trend of increasing gross thrust coefficient with increasing secondary flow existed over the Mach number range for both configurations. Assessing the nozzle for the ram drag penalty of the secondary flow (performance parameter, $[(F - D) - m_s V_0]/F_{i,p}$) also resulted in an increasing trend with increasing secondary flow (fig. 17). However, penalizing the nozzle for the ram drag of the secondary flow causes the performance to be less sensitive to corrected secondary weight flow.

Figure 18 shows the effect of corrected secondary weight flow ratio on the nozzle pumping characteristics for various flight Mach numbers and nozzle pressure ratios both with and without sideplates. The pumping characteristics of both configurations were approximately the same.

Pressure Distributions

Pressure distributions over the nozzle assembly are shown in figures 19 to 22 for both wedge nozzle configurations. These data are shown for various Mach numbers and a nominal corrected secondary weight flow of 4 percent. Figure 19 shows the pressure distribution along the shroud boattail and primary flap for the retracted shroud without sideplates. Pressure taps on the shroud boattail were located at $x/l = -0.297$ and circumferentially at 15° increments (to facilitate their presentation) an average pressure coefficient is presented. The average pressure coefficient was taken from 315° to 45° , 45° to 135° , 135° to 225° , and 225° to 315° .

There was a circumferential pressure gradient on the external shroud over the Mach range tested. In general, the peak average pressure coefficient occurred near

the top (315° to 45°), and the minimum pressure coefficient occurred near the bottom (135° to 225°). The 315° to 45° position indicates the effect of the wing flow field, which tends to create the positive installation effect. A comparison of figures 19(a) to (g) shows the effect of the local flow field over the Mach number range on both the external shroud and primary flap.

The pressure distributions on the shroud boattail and along the primary flap for the retracted shroud with sideplates are shown in figure 20. The pressures on the external shroud were measured at $x/l = -0.268$. The trends for this configuration were generally the same as those for the retracted shroud without sideplates. However, the minimum pressure coefficient on the shroud with sideplates was considerably lower than the pressure coefficient for configuration without sideplates. This effect is a result of the external shape of the sideplate configuration.

The static-pressure distribution along the wedge surface is presented in figures 21 and 22 for the retracted shroud with and without sideplates. Static pressure measurements were made on both sides of the wedge, along the centerline, and 16.82 centimeters (6.62 in.) off center. The reciprocal of P_g/p_0 , the nozzle pressure ratio, is shown in each figure. The data above this line represent a thrust, and those below a drag force. The axial pressure distribution is similar to that for a plug nozzle; that is, there occurs to the flow an initial overexpansion followed by a recompression above ambient. The entire process is then repeated.

The initial pressure along the wedge centerline was higher than that at the wedge sides. However, the pressure along the centerline expands (initially) to a lower pressure than that at the 16.82-centimeter (6.62-in.) off center location. As the Mach number (and nozzle pressure ratio) increases beyond 0.95 (figs. 21(f) and (g)), a large segment of the wedge is under the influence of a drag force. This is a result of terminal shock which has moved aft of the nozzle assembly.

The static-pressure distribution along the wedge surface for the retracted shroud with sideplates is shown in figure 22 for Mach numbers of 0.80, 0.84, and 0.90. The trends of this configuration were the same as those for the shroud without sideplates. These results are expected since the sideplates shield a very small portion of the wedge surface.

Comparisons of Secondary Flow Effect on Wedge and Plug

Nozzle Performance Characteristics

Schematics of the plug nozzles are shown in figure 23. A comparison of the effect of secondary flow on the nozzle gross thrust coefficient for the wedge and plug nozzles is presented in figure 24 for various flight Mach numbers and nozzle pressure ratios. The wedge and boattail nacelle plug nozzles had about the same level of performance over the secondary weight flow range (0.02 to 0.09). However, the cylindrical nacelle plug nozzle was about 2 percent lower at both $M_0 = 0.80$ and 0.90 over the secondary flow range.

Assessing the nozzles for the ram drag penalty of the secondary flow (performance parameter, $[(F - D) - m_0 V_s / F_{ip}]$) resulted in an increasing trend with increasing secondary flow (fig. 25). However, the performance parameter is less sensitive to corrected secondary weight flow than the nozzle gross thrust coefficient for all three nozzles.

The effect of secondary weight flow on the pumping characteristics is shown in figure 26 for Mach 0.80 and 0.90. The wedge nozzle required a slightly higher secondary pressure level to obtain the same percentage of weight flow as the cylindrical nacelle plug nozzle. The secondary-flow pumping characteristics were about the same for both wedge and boattail nacelle plug nozzles.

A comparison of the secondary-flow effect on the component force is presented in figure 27 at flight Mach 0.90 for the wedge and plug nozzles. Because of instrumentation limitations, the wedge nozzle was not sufficiently instrumented to give an accurate account of the forces on all component surfaces. For example, the wedge sides, which have a slight divergence, were not instrumented.

The primary momentum of the wedge nozzle was about the same as the boattail nacelle plug nozzle both of which were higher than the cylindrical nacelle plug nozzle. The centerbody area-to-nacelle area was 0.52 for the wedge nozzle; 0.26 for the boattail nacelle and 0.46 for the cylindrical nacelle plug nozzle. However, the cylindrical nacelle plug nozzle had a slightly higher centerbody component thrust than the wedge. This difference could be the result of insufficient instrumentation on the wedge to give a more precise account of the distorted flow in the spanwise direction (shown in fig. 21). Nevertheless, an increase in secondary flow had an insignificant effect on the nozzle centerbody pressure forces.

The secondary momentum for both the wedge and boattail nacelle nozzles produced a thrust over the secondary-flow range. However, such was not the case for the cylindrical nacelle plug nozzle at a secondary weight flow below 4.5 percent where the secondary total pressure was less than p_0 . Other components of the wedge nozzle had such small areas where the forces were approximately zero.

SUMMARY OF RESULTS

A flight investigation was conducted to determine the installation effects on a wedge nozzle that was designed for subsonic-low supersonic speeds. This research program was conducted with an F-106B aircraft modified to carry two underwing nacelles. The investigation was made over a Mach number range of 0.70 to 1.10, and the results were compared with an isolated, cold-flow, wedge nozzle configuration and an installed boattail and cylindrical nacelle plug nozzles at subsonic speeds. Data were also obtained over a secondary flow range at selected flight Mach numbers and partial power. The following results were obtained.

1. The installed wedge nozzle with a retracted external shroud had a favorable installation effect from Mach 0.82 to about 0.96. The peak difference in gross thrust coefficient was 0.053 which occurred at Mach 0.95 (0.966 and 0.913 for the installed and isolated wedge nozzle, respectively).

2. The nozzle gross thrust coefficient of the wedge nozzle (retracted shroud without sideplates) was about the same as the best installed plug nozzle results (boattail nacelle plug) over the subsonic Mach number range. The wedge nozzle gross-thrust coefficient was significantly higher than that of the cylindrical nacelle plug nozzle over the subsonic Mach number range.

3. At Mach numbers of 0.80 and 0.90 and 4 percent secondary flow ratio, a retracted external shroud configuration without sideplates had about a 1-percent higher gross thrust coefficient than a configuration with sideplates. At a higher corrected secondary weight flow (8 percent), there was a slight but insignificant difference in gross thrust coefficient of the two configurations.

Lewis Research Center,
National Aeronautics and Space Administration,
Cleveland, Ohio, December 12, 1974,
505-04.

REFERENCES

1. Crabs, Clifford C.; Mikkelson, Daniel C.; and Boyer, Earle O.: An Inflight Investigation of Airframe Effects on Propulsion System Performance at Transonic Speeds. Presented at the 13th Annual Symposium of the Society of Experimental Test Pilots, Los Angeles, Calif., Sept. 25-27, 1969.
2. Nichols, Mark R.: Aerodynamics of Airframe-Engine Integration of Supersonic Aircraft. NASA TN D-3390, 1966.
3. Barley, Richard R.: Flight Investigation of Airframe Installation Effects on an Auxiliary Inlet Ejector Nozzle on an Underwing Engine Nacelle. NASA TM X-2396, 1971.
4. Mikkelson, Daniel C.; and Head, Verlin L.: Flight Investigation of Airframe Installation Effects on a Variable Flap Ejector Nozzle of an Underwing Engine Nacelle at Mach Numbers from 0.5 to 1.3. NASA TM X-2010, 1970.
5. Samanich, Nick E.; and Chamberlin, Roger: Flight Investigation of Installation Effects on a Plug Nozzle Installed on an Underwing Nacelle. NASA TM X-2295, 1971.
6. Johns, Albert L.; and Jeracki, Robert J.: Preliminary Investigation of Performance of a Wedge Nozzle Applicable to a Supersonic-Cruise Aircraft. NASA TM X-2169, 1970.
7. Johns, Albert L.: Internal Performance of a Wedge Nozzle for a Supersonic-Cruise Aircraft with a Multispoke Primary for Noise Suppression. NASA TM X-2689, 1972.
8. Groth, Harold W.; Samanick, Nick E.; and Blumenthal, Philip Z.: Inflight Thrust Measuring System for Underwing Nacelles Installed on a Modified F-106 Aircraft. NASA TM X-2356, 1971.
9. Burley, Richard R.; Karabinus, Raymond J.; and Freedman, Robert J.: Flight Investigation of Acoustic and Thrust Characteristics of Several Exhaust Nozzles Installed on Underwing Nacelles on an F-106 Airplane. NASA TM X-2854, 1973.

10. Antl, Robert J.; and Burley, Richard R.: Steady-State Airflow and After-burning Performance Characteristics of Four J85-GE-13 Turbojet Engines. NASA TM X-1742, 1969.
11. Blaha, Bernard J.; and Bresnahan, Donald L.: Wind Tunnel Installation Effects on Isolated Afterbodies at Mach Numbers from 0.56 to 1.5. NASA TM X-52581, 1969.
12. Head, Verlon L.: Flight Investigation of Installation Effects on a Plug Nozzle with a Series of Boattailed Primary Shroud Installed on an Underwing Nacelle on an F-106 Airplane. NASA TM X-2983, 1973.

TABLE I. - COORDINATES OF WEDGE SURFACE

UPSTREAM OF STATION 8^a

S station		b _T ±		S station		b _T ±	
cm	in.	cm	in.	cm	in.	cm	in.
0	0	15.11	5.95	25.40	10.00	9.98	3.93
2.69	1.06	15.49	6.10	27.94	11.00	8.74	3.44
3.81	1.50	15.67	6.17	30.48	12.00	7.39	2.91
5.08	2.00	15.80	6.22	31.12	12.25	7.04	2.77
6.35	2.50	15.85	6.24	31.75	12.50	6.63	2.61
7.62	3.00	15.82	6.23	32.38	12.75	6.22	2.45
8.89	3.50	15.72	6.19	33.02	13.00	5.79	2.28
10.16	4.00	15.49	6.10	33.66	13.25	5.31	2.09
11.43	4.50	15.19	5.98	34.29	13.50	4.78	1.88
12.70	5.00	14.81	5.83	34.92	13.75	4.17	1.64
15.24	6.00	14.02	5.52	35.56	14.00	3.48	1.37
17.78	7.00	13.11	5.16	36.20	14.25	2.67	1.05
20.32	8.00	12.14	4.78	36.83	14.50	1.32	.52
22.86	9.00	11.10	4.37	37.03	14.58	0	0

^aSee fig. 5.^bCoordinates are faired smoothly.

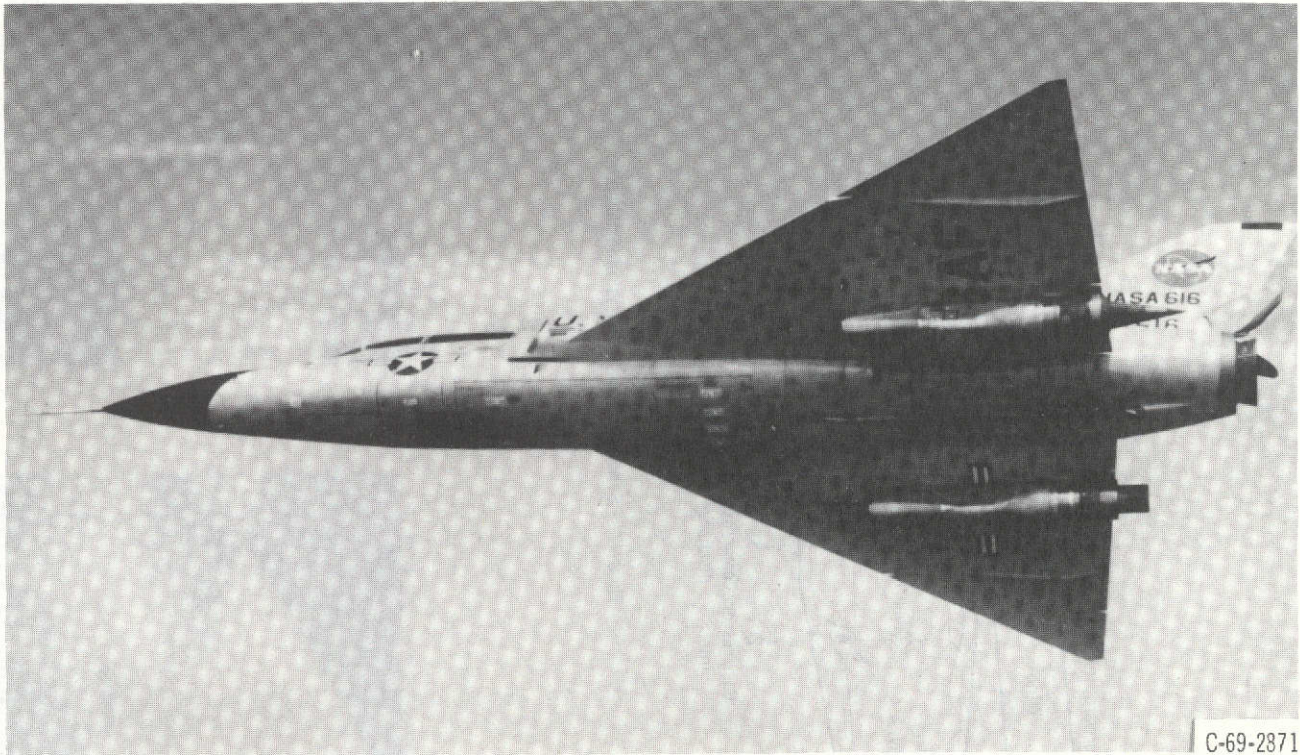
TABLE II. - NOZZLE PROJECTED AREA RATIOS

Nozzle	Primary flap area-to- nacelle area	Boattail area-to- nacelle area	Centerbody area-to- nacelle area
Wedge	0.03	0.12	0.52
Boattailed nacelle plug ^a	.32	.19	.26
Cylindrical nacelle plug ^a	.20	0	.46

^aRef. 5.

ORIGINAL PAGE IS
OF POOR QUALITY

ORIGINAL PAGE IS
OF POOR QUALITY



C-69-2871

Figure 1. - Modified F-106B aircraft in flight, showing underwing installation of nozzles.

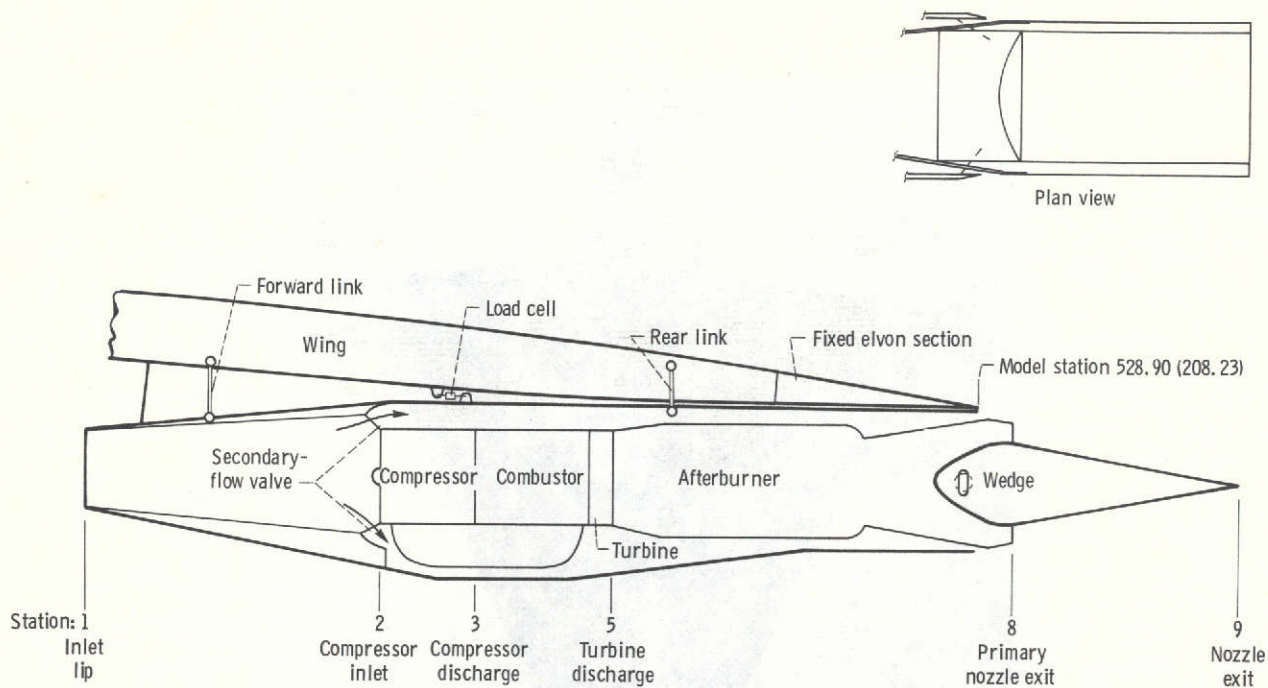
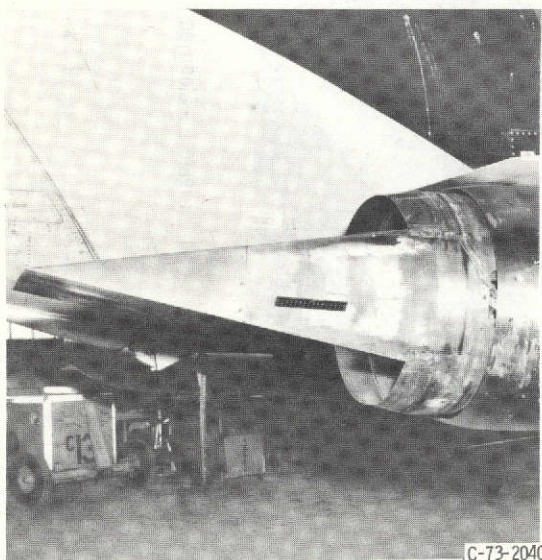
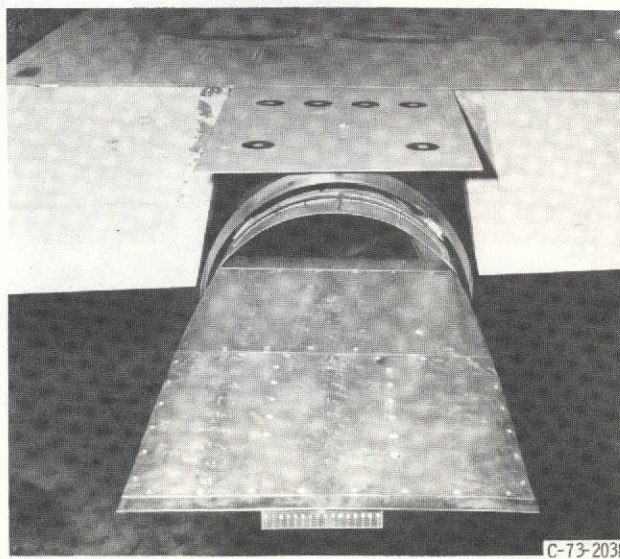


Figure 2. - Schematic of nacelle-engine installation.

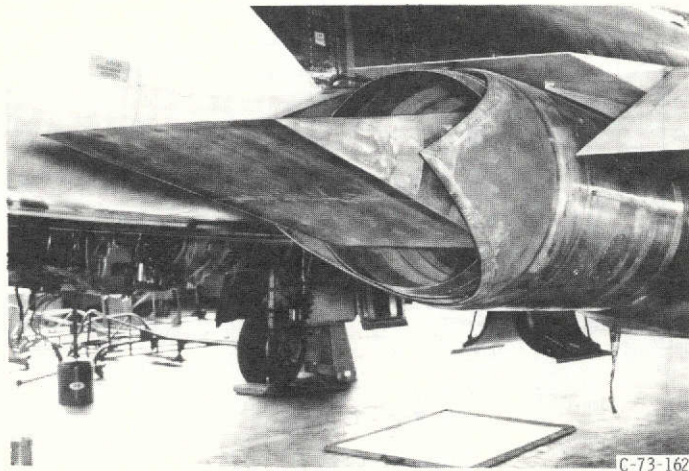


(a) Three-quarter side view.

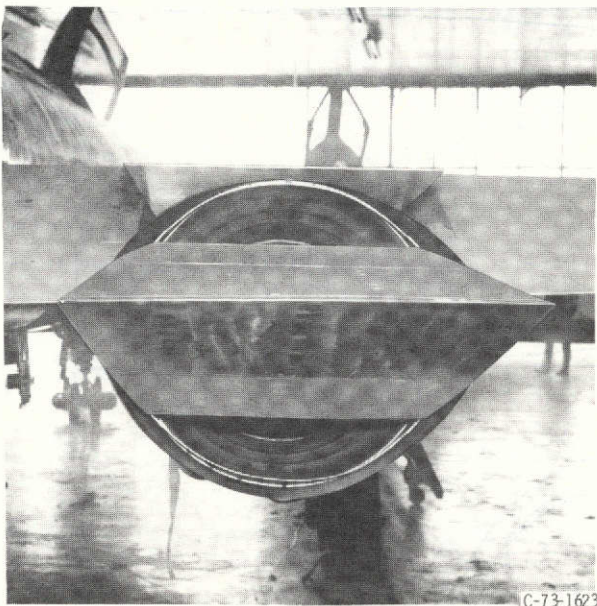


(b) Three-quarter top view.

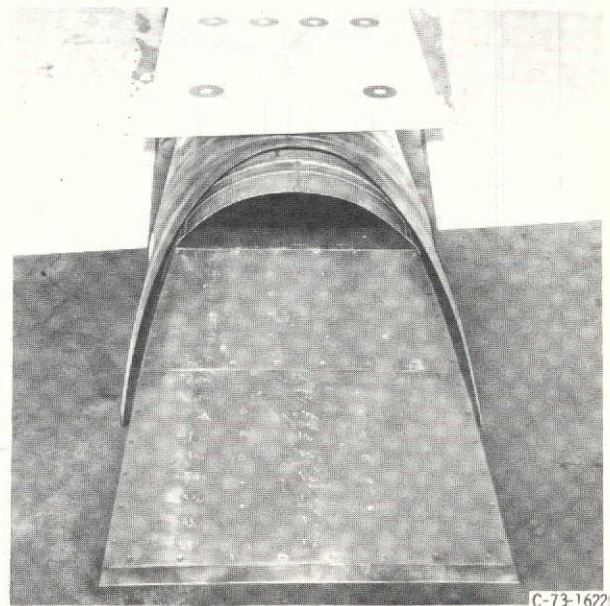
Figure 3. - Retracted shroud without sideplates. Shroud extension, x/l , -0.231 .



(a) Three-quarter aft view.



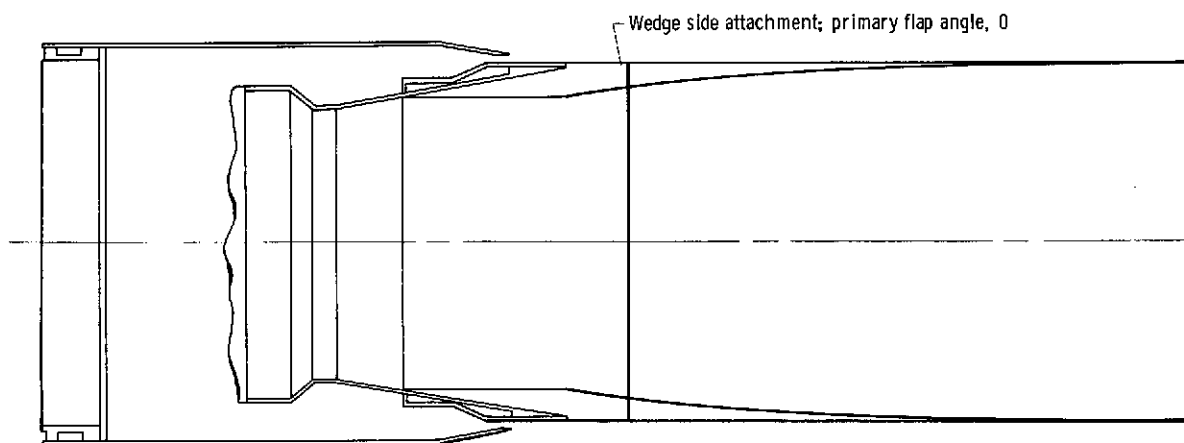
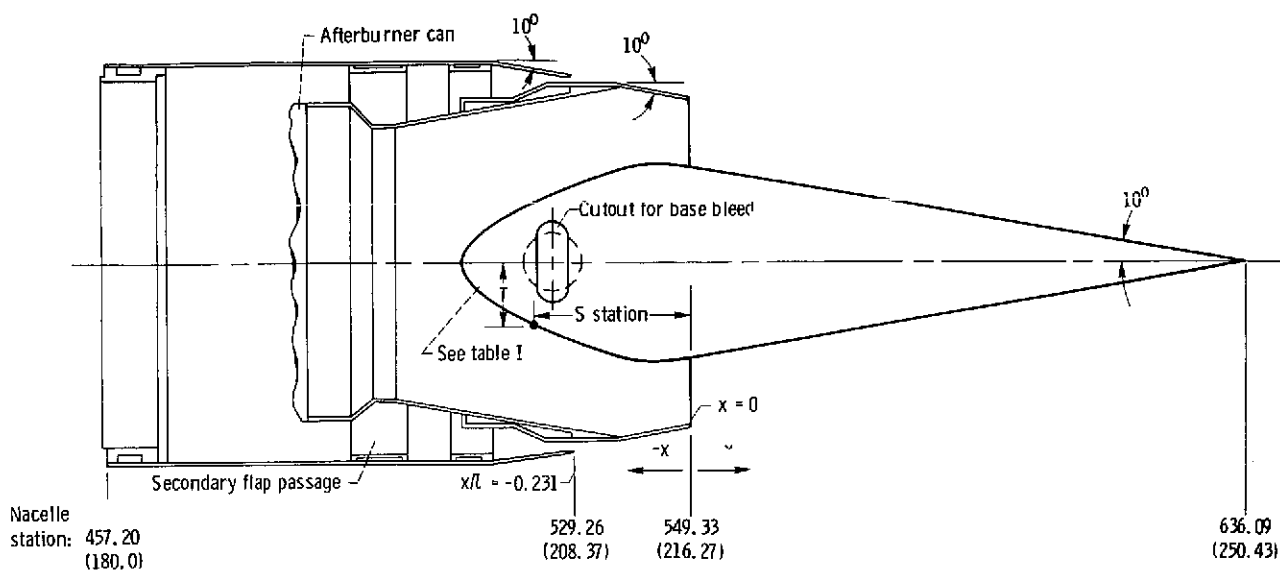
(b) Aft view.



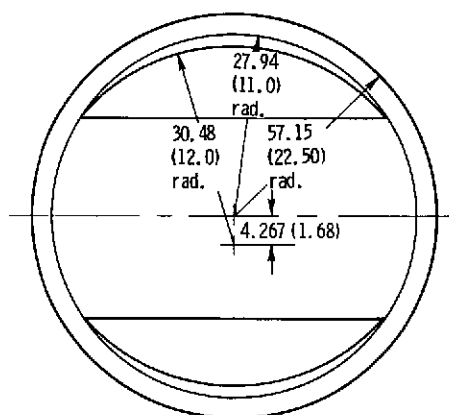
(c) Three-quarter top view.

Figure 4. - Retracted shroud with sideplates. Shroud extension, x/l , -0.236 .

ORIGINAL PAGE IS
OF POOR QUALITY

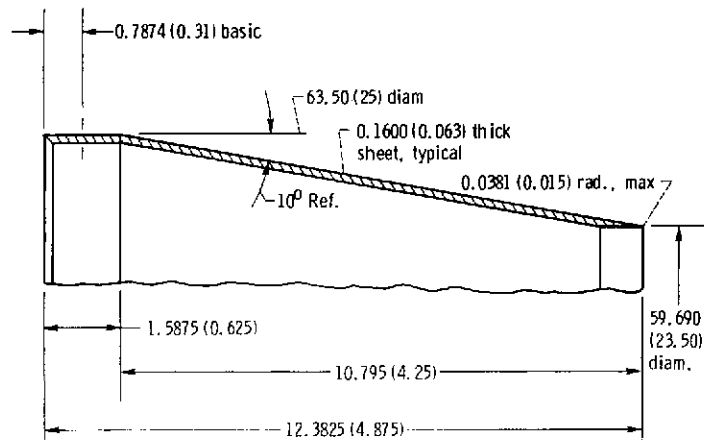


Top view

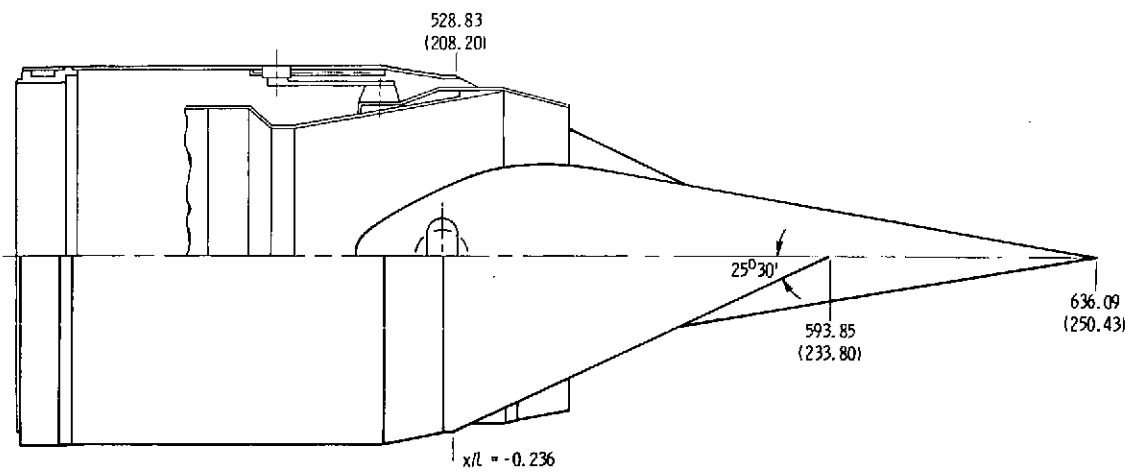
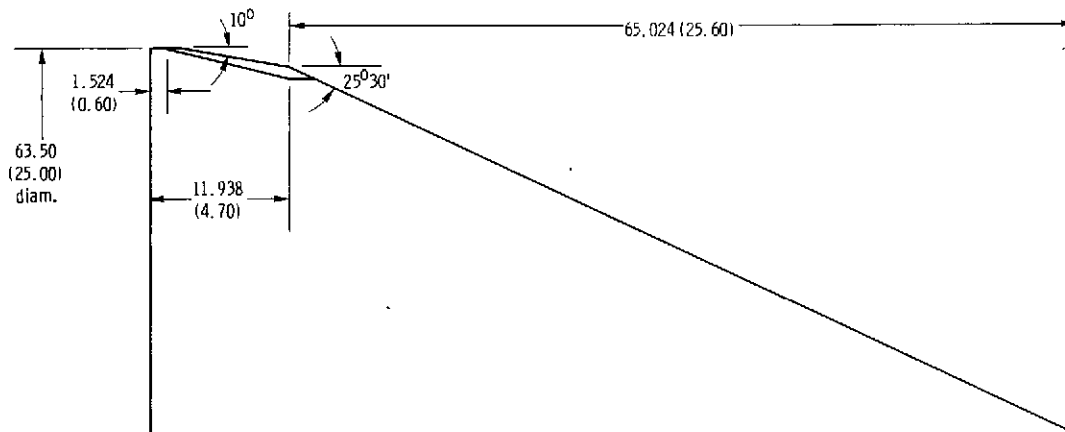


(a) Retracted external shroud without sideplates.

Figure 5. - Wedge nozzle dimensions. (All dimensions are in cm (in.)).



Details of external shroud



(b) Retracted external shroud with sideplates.

Figure 5. - Concluded.

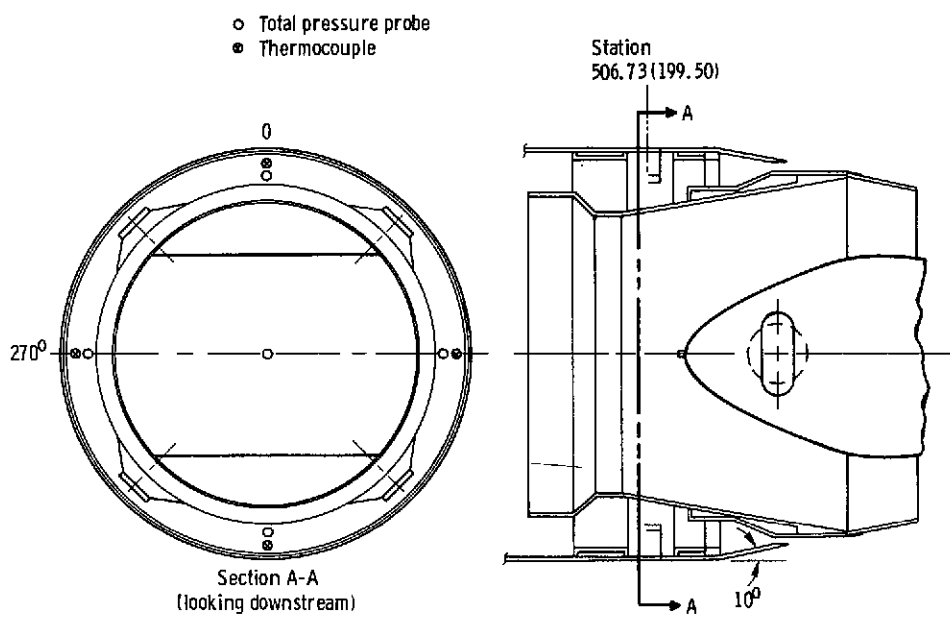
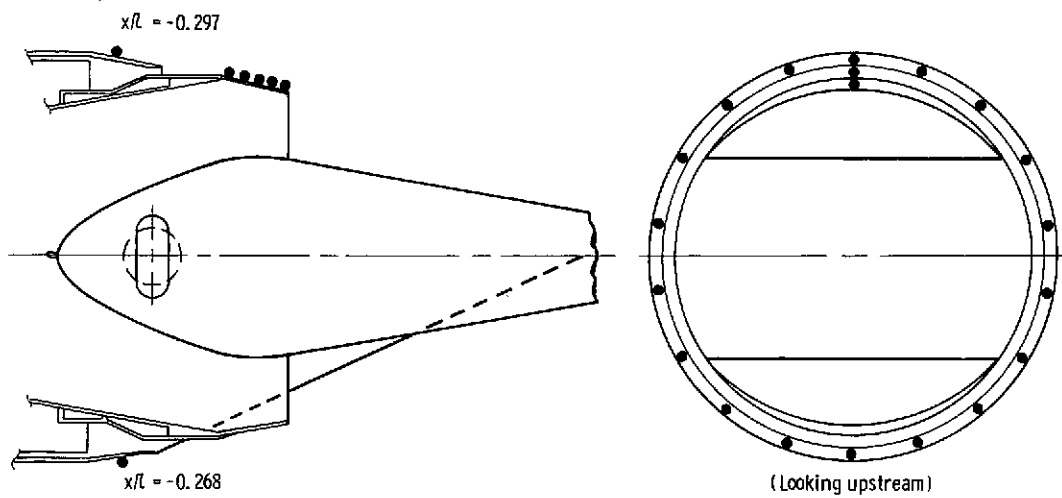
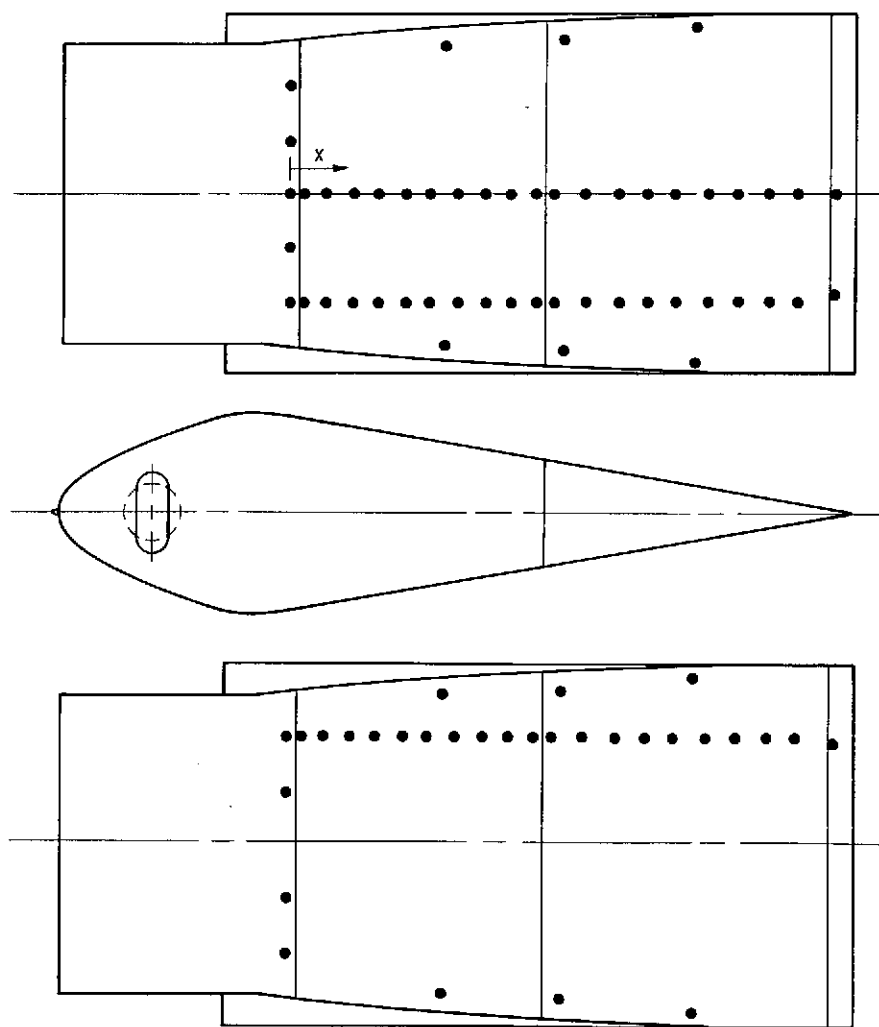


Figure 6. - Secondary passage instrumentation. (All dimensions are in cm (in.).)



(a) External shroud and primary nozzle static pressures.



(b) Wedge static pressures.

Figure 7. - Nozzle instrumentation.

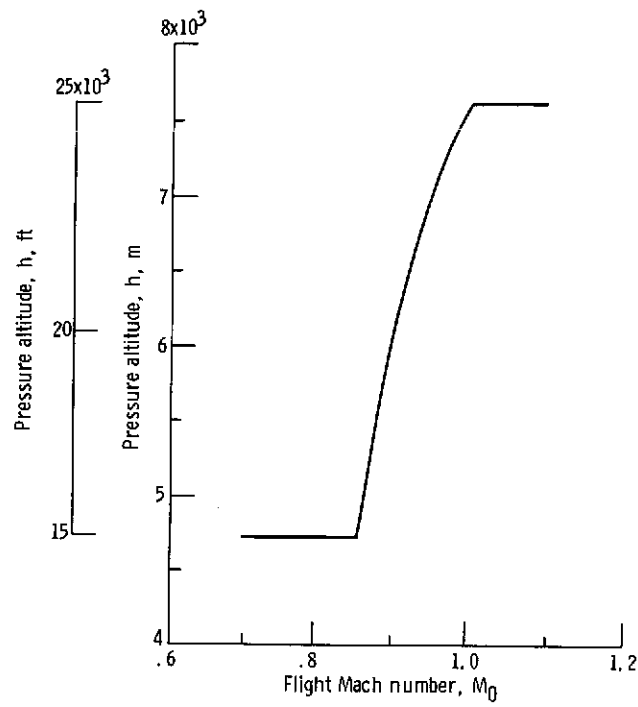


Figure 8. - Nominal flight test altitude - Mach number profile.

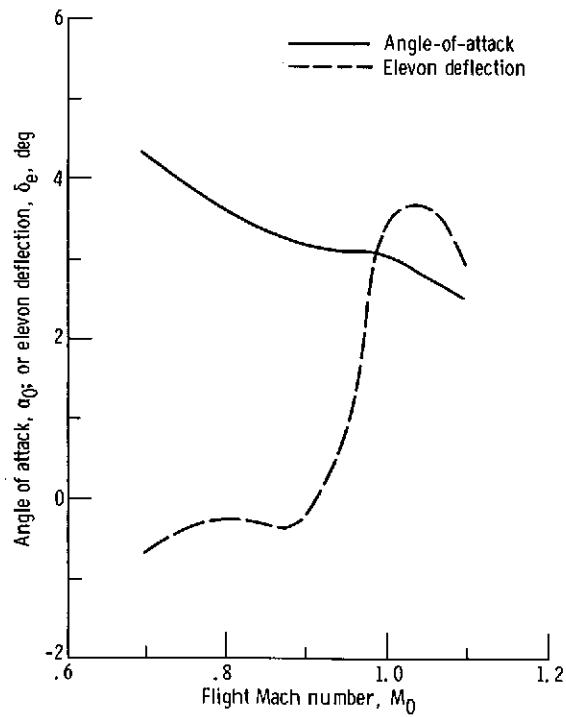


Figure 9. - Nominal angle-of-attack and elevon deflection with nacelles installed.

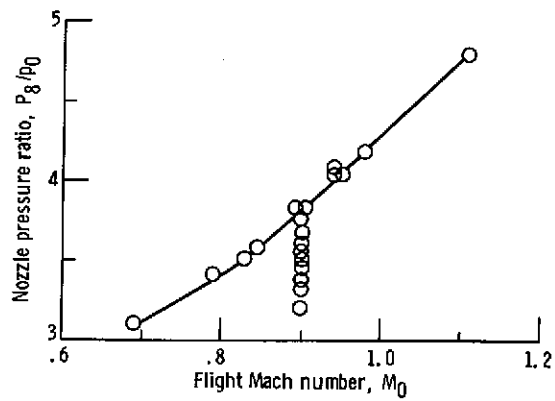


Figure 10. - Nozzle pressure ratio - flight Mach number schedule.

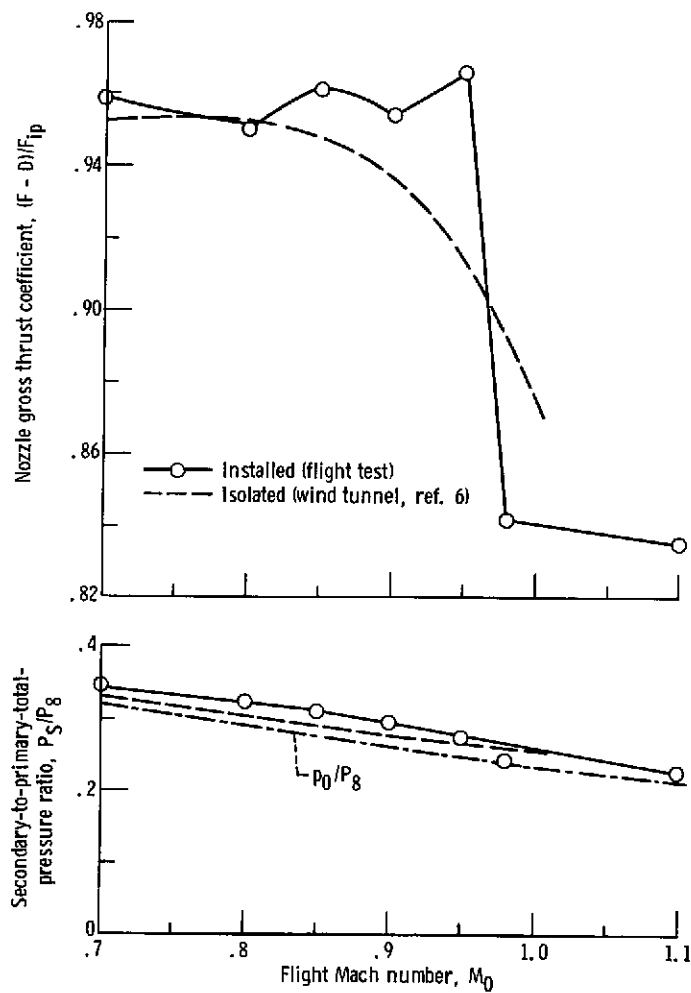


Figure 11. - Installation effect on nozzle performance characteristics. Retracted shroud without sideplates; nominal corrected secondary weight flow, 0.04.

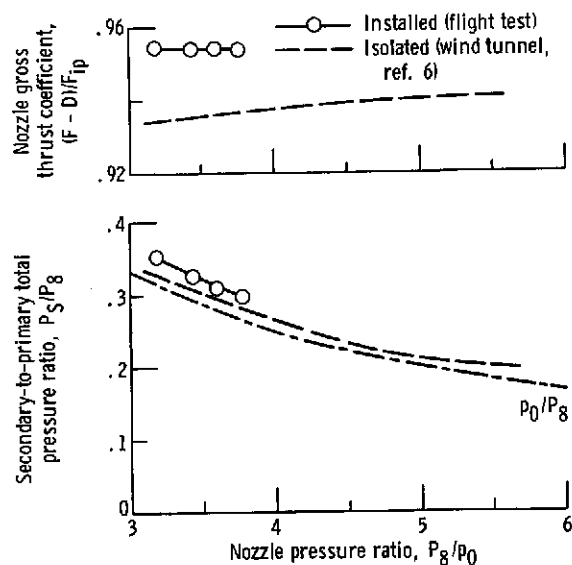


Figure 12. - Installation effect on nozzle performance characteristics. Mach 0.9; retracted shroud without sideplates; nominal corrected secondary weight flow, 0.04.

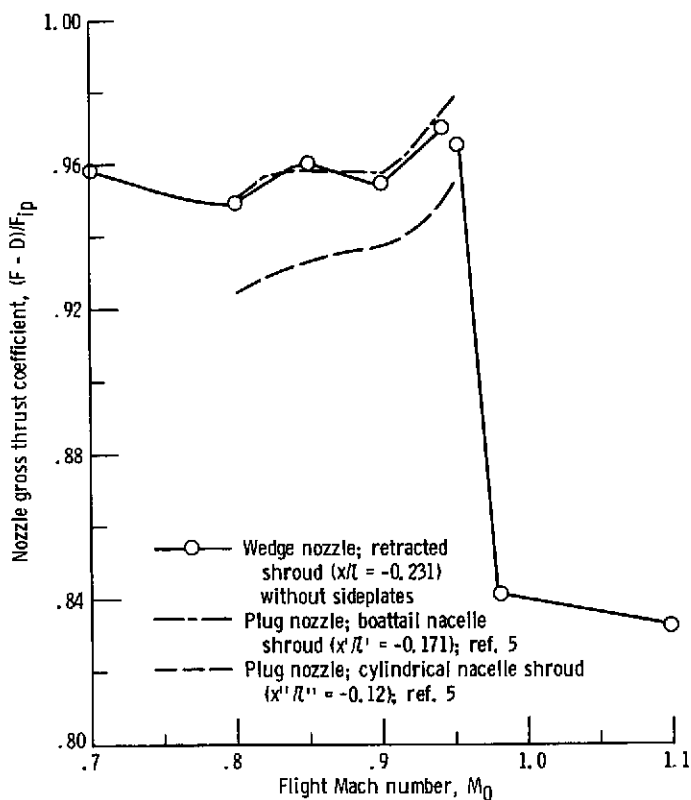


Figure 13. - Comparison of wedge nozzle to plug nozzle at military power setting. Nominal corrected secondary weight flow ratio, 0.04.

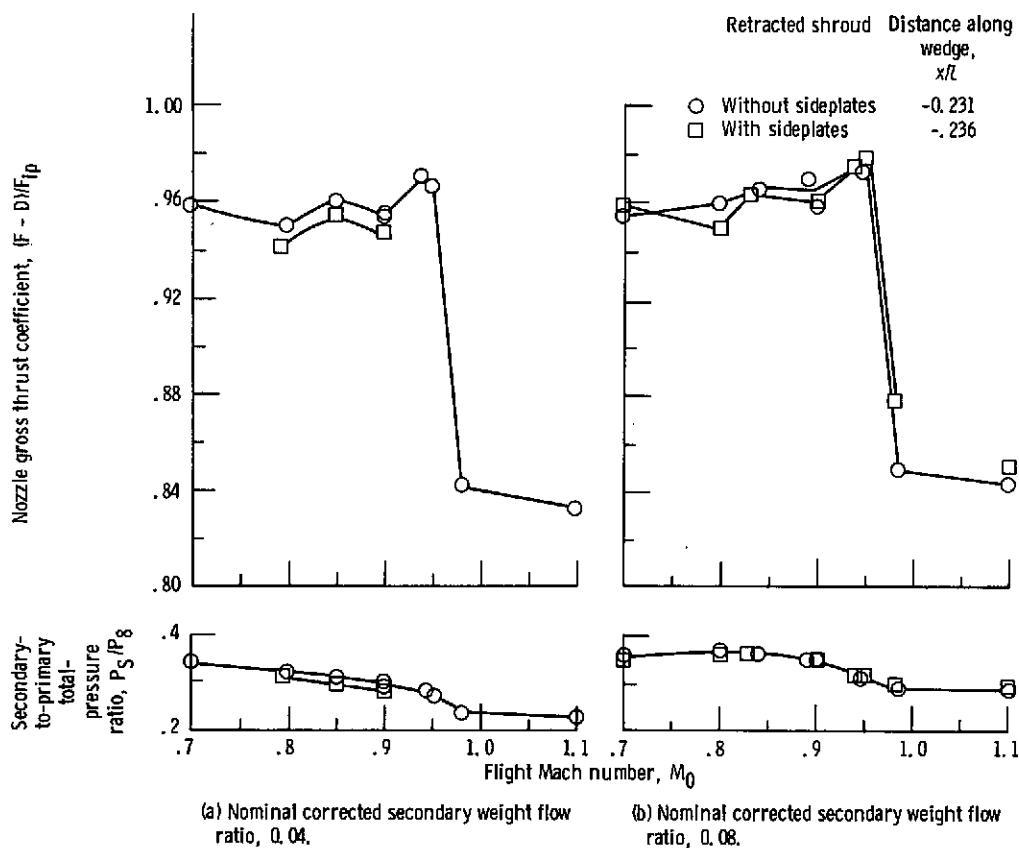


Figure 14. - Comparison of installed performance with and without sideplates.

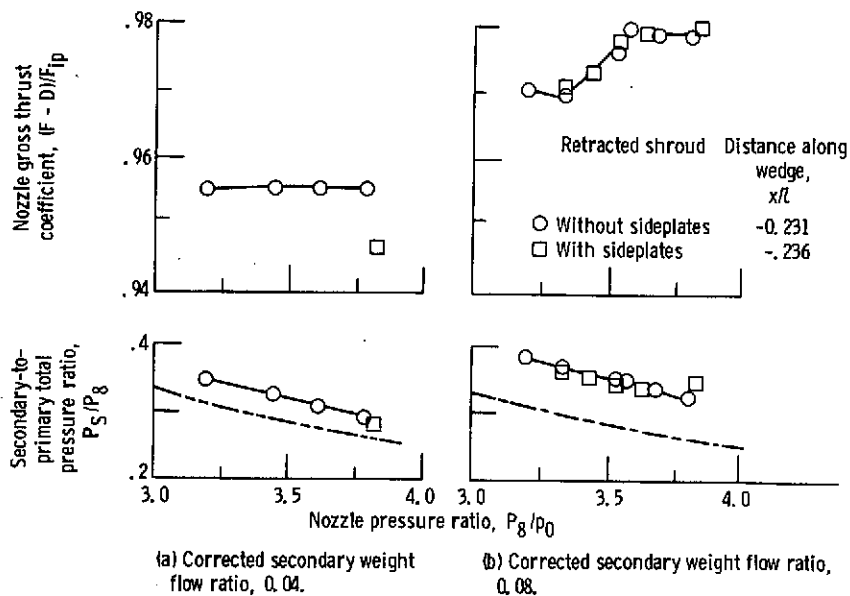


Figure 15. - Comparison of effect of nozzle pressure ratio on installed nozzle performance characteristics at flight Mach 0.90.

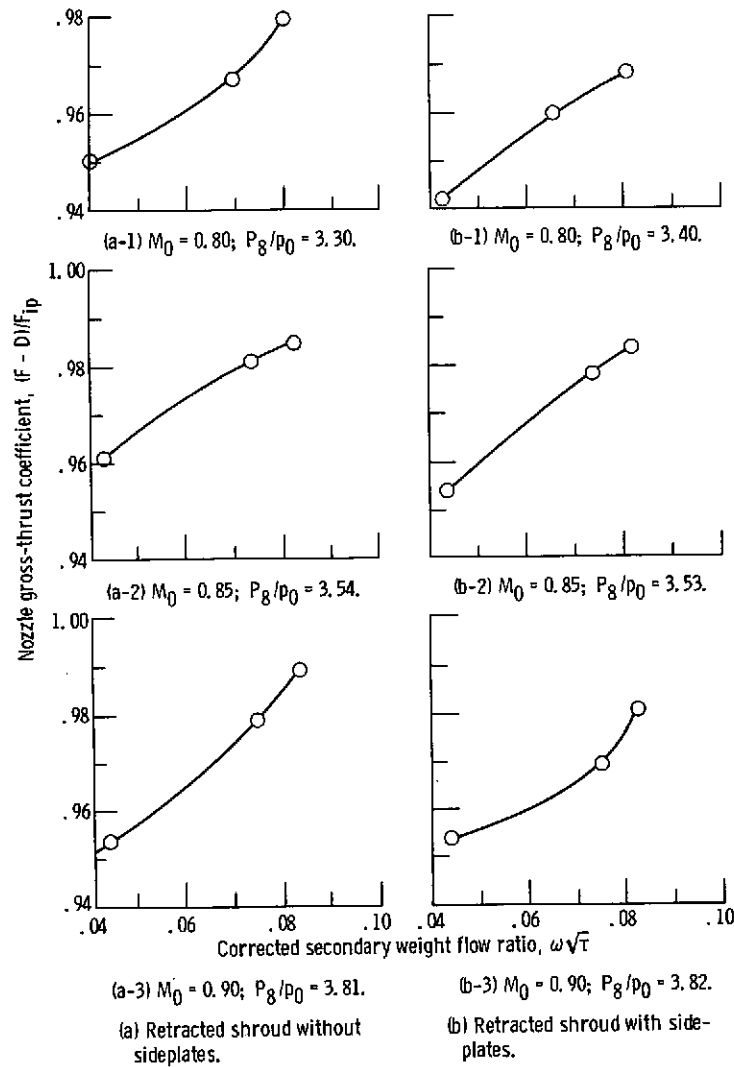


Figure 16. - Effect of secondary flow on nozzle gross thrust coefficient for various flight Mach numbers M_0 and nozzle pressure ratios P_g/p_0 .

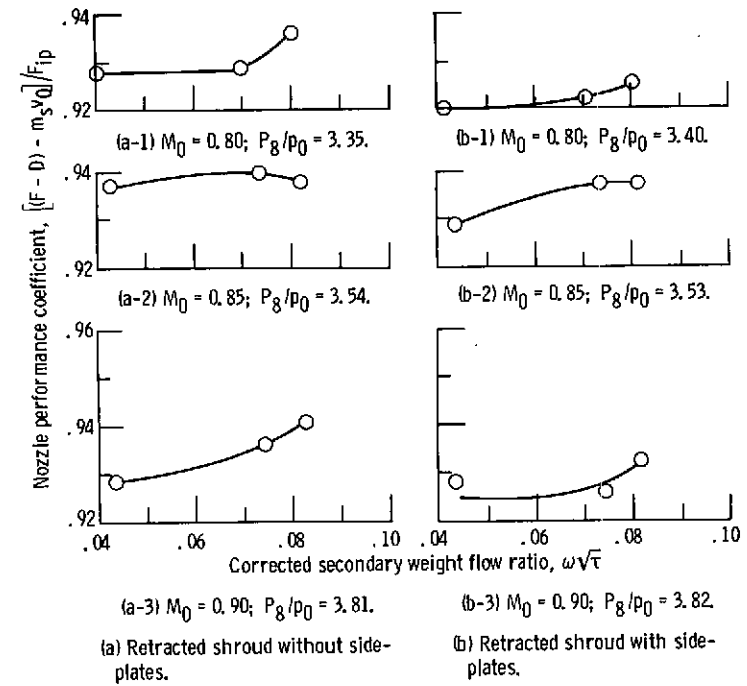


Figure 17. - Effect of secondary flow on nozzle performance coefficient for various flight Mach numbers M_0 and nozzle pressure ratios P_g/p_0 .

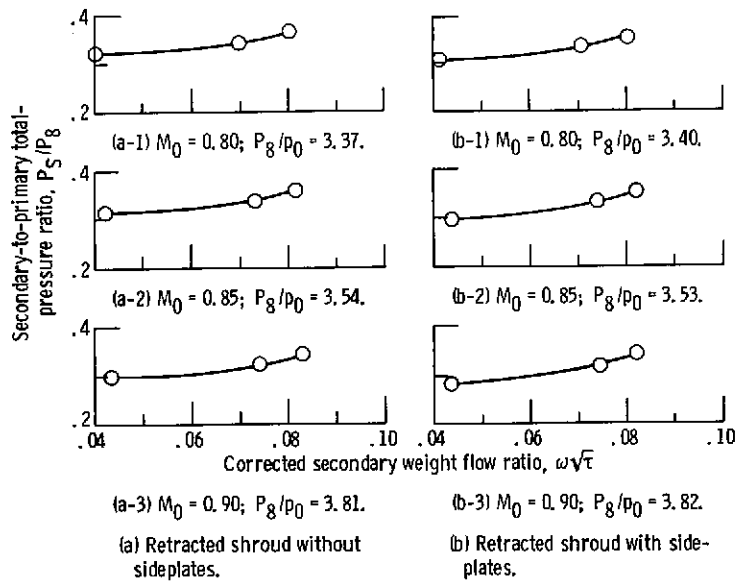


Figure 18. - Effect of secondary weight flow on secondary-to-primary total-pressure ratio for various flight Mach numbers M_0 and nozzle pressure ratios P_8/p_0 .

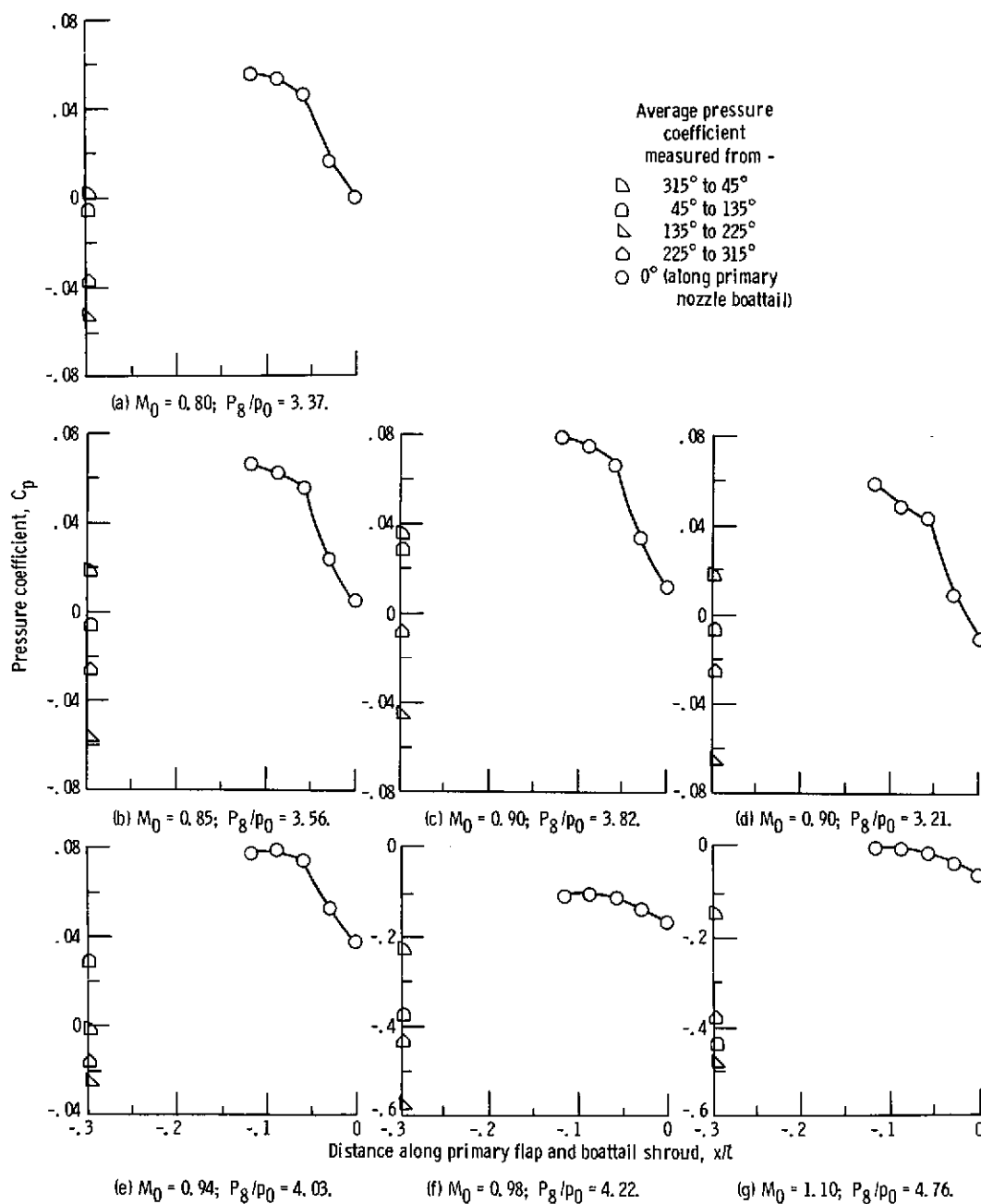


Figure 19. - Pressure distribution along boattail shroud and primary flap of the retracted shroud without side-plates for flight Mach numbers M_0 and nozzle pressure ratios P_g/p_0 . Corrected secondary weight flow, 0.042.

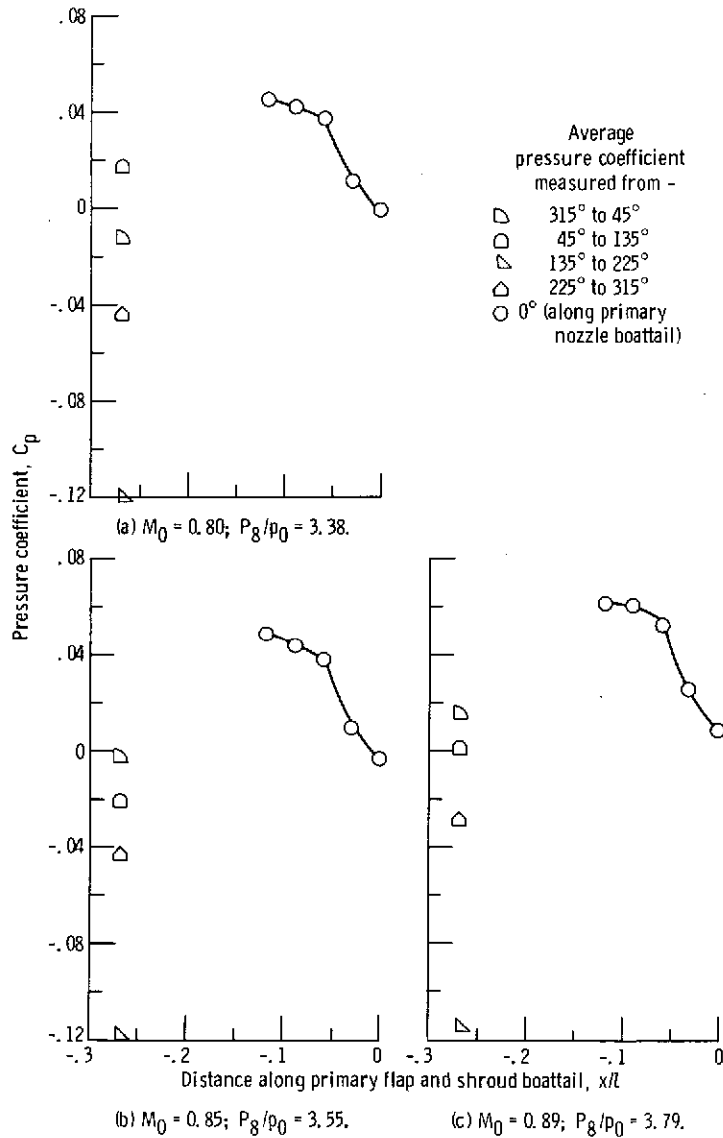


Figure 20. - Pressure distribution along shroud boattail and primary flap of retraced shroud with sideplate for flight Mach numbers M_0 and nozzle pressure ratios P_g/p_0 . Corrected secondary weight flow, 0.042.

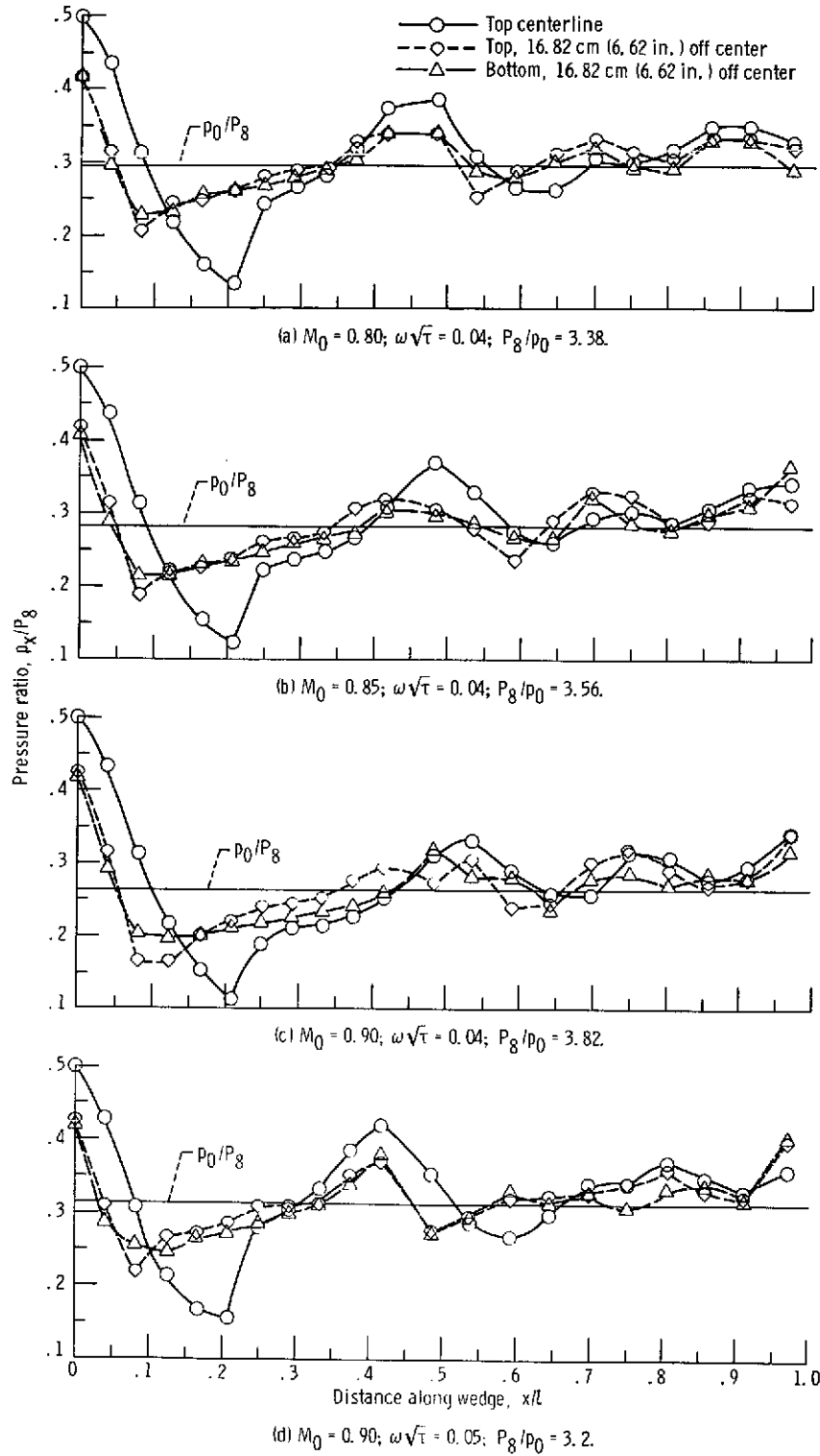


Figure 21. - Static-pressure distribution on wedge surface for flight Mach number M_0 , corrected secondary weight flow ratios $\omega\sqrt{\tau}$, and nozzle pressure ratios P_8/p_0 . External shroud without sideplates.

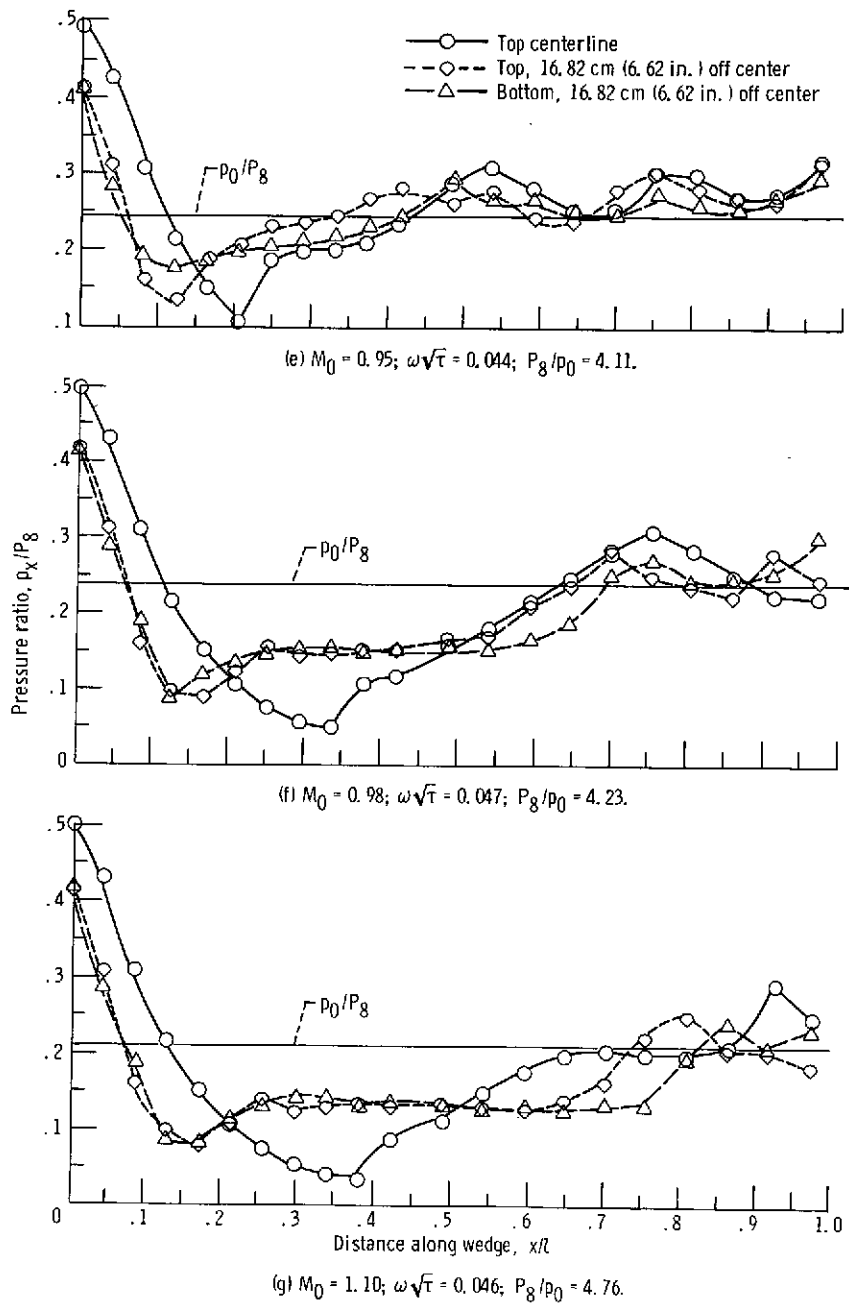


Figure 21. - Concluded.

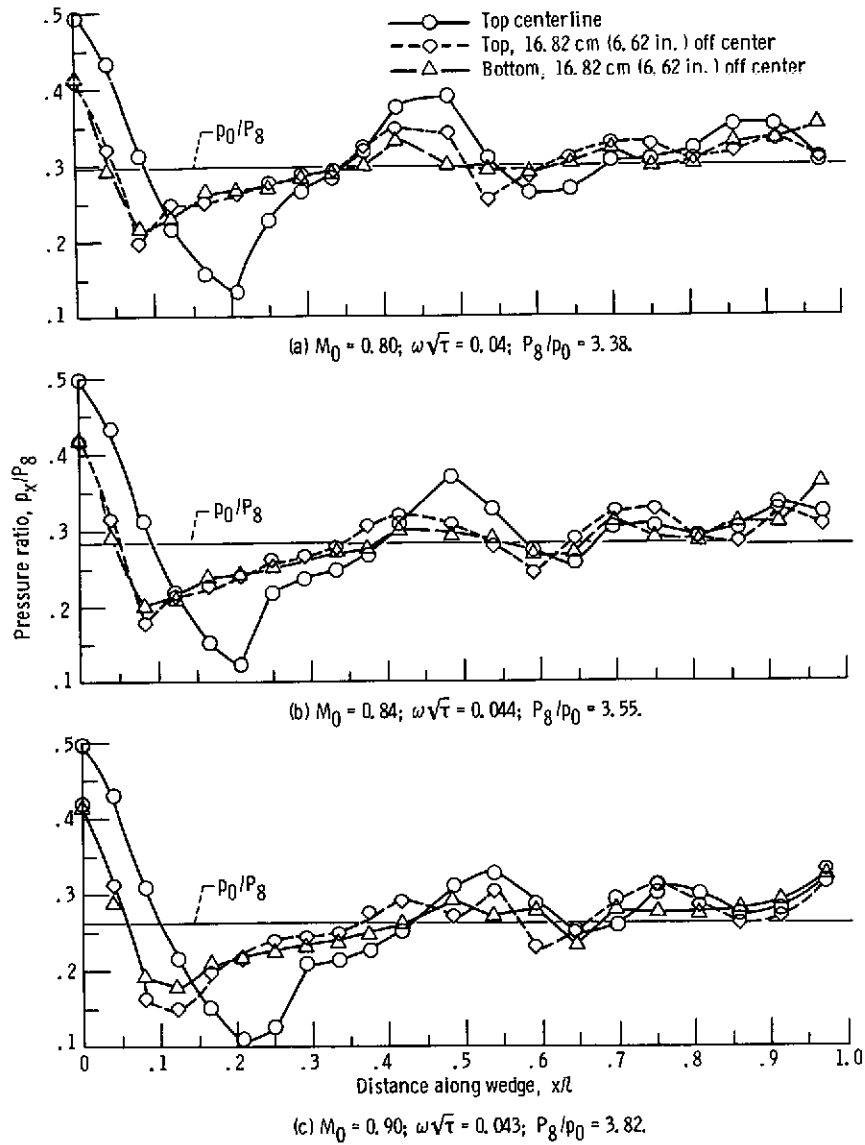


Figure 22. - Static pressure distribution on wedge surface for flight Mach numbers M_0 , corrected secondary weight flow ratios, $\omega\sqrt{\tau}$, and nozzle pressure ratios, P_8/p_0 .

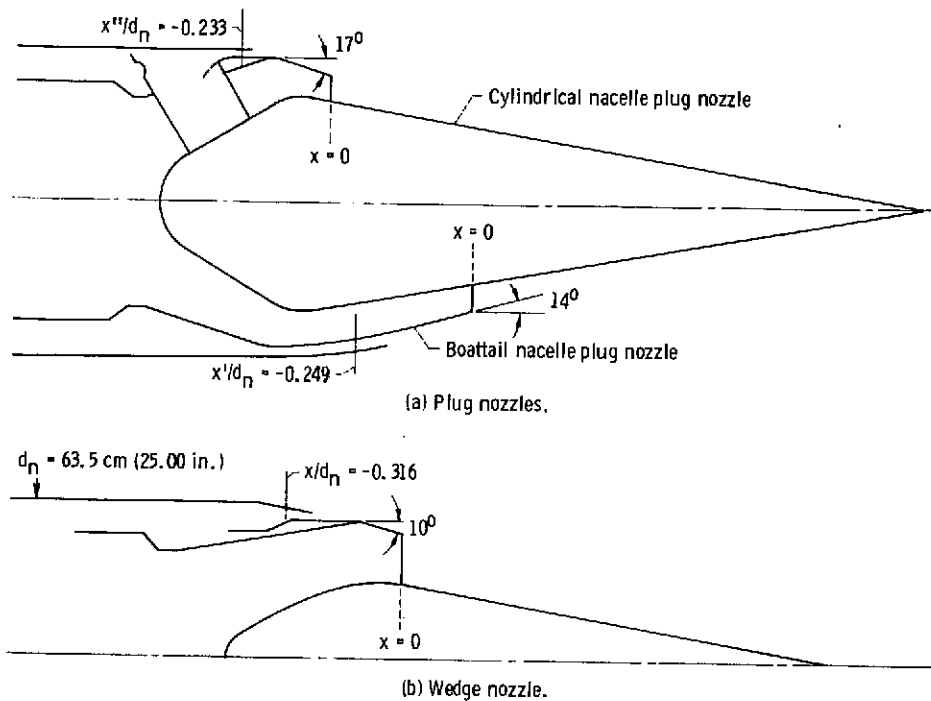


Figure 23. - Plug nozzles studied.

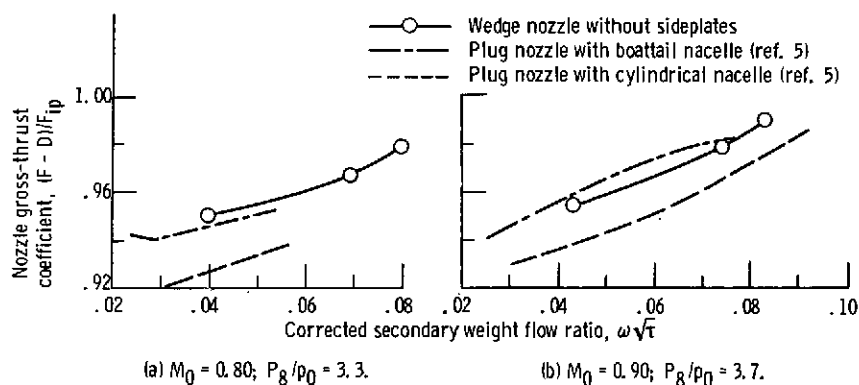


Figure 24. - Comparison of the effect of secondary flow on nozzle gross-thrust coefficient for wedge nozzle ($x/d_n = -0.316$), boattail nacelle plug nozzle ($x'/d_n = -0.249$) and cylindrical nacelle plug nozzle ($x''/d_n = -0.233$) at various flight Mach numbers M_0 and nozzle pressure ratios P_g/p_0 .

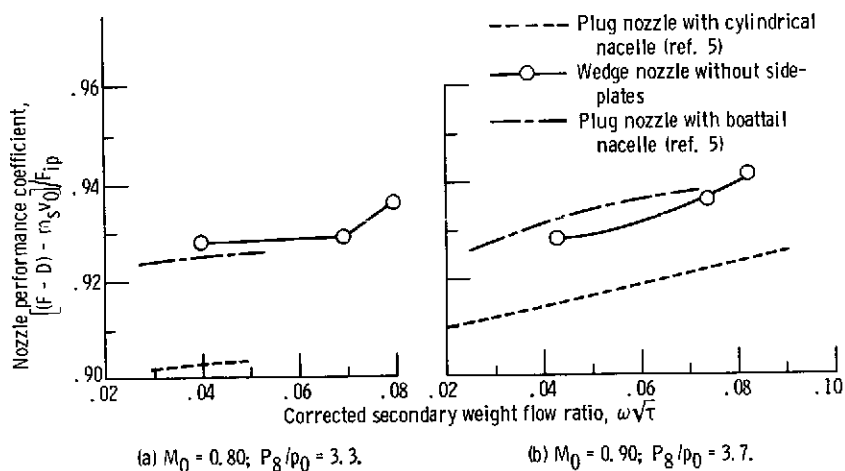


Figure 25. - Comparison of effect of secondary flow on nozzle performance coefficient for the wedge nozzle, and boattail and cylindrical nacelle plug nozzles at various flight Mach numbers M_0 and nozzle pressure ratios P_8/p_0 .

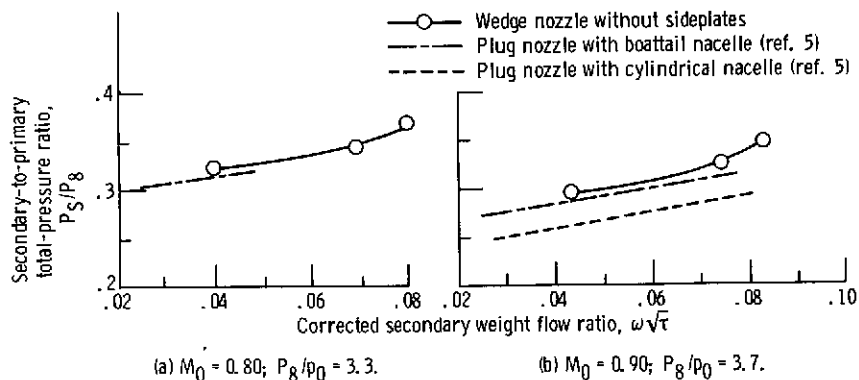


Figure 26. - Comparison of effect of secondary flow on secondary-to-primary total-pressure ratio for wedge nozzle ($x/d_n = -0.316$); boattail nacelle plug nozzle ($x'/d_n = -0.249$), and cylindrical nacelle plug nozzle ($x''/d_n = -0.233$) at various flight Mach numbers M_0 and nozzle pressure ratios P_8/p_0 .

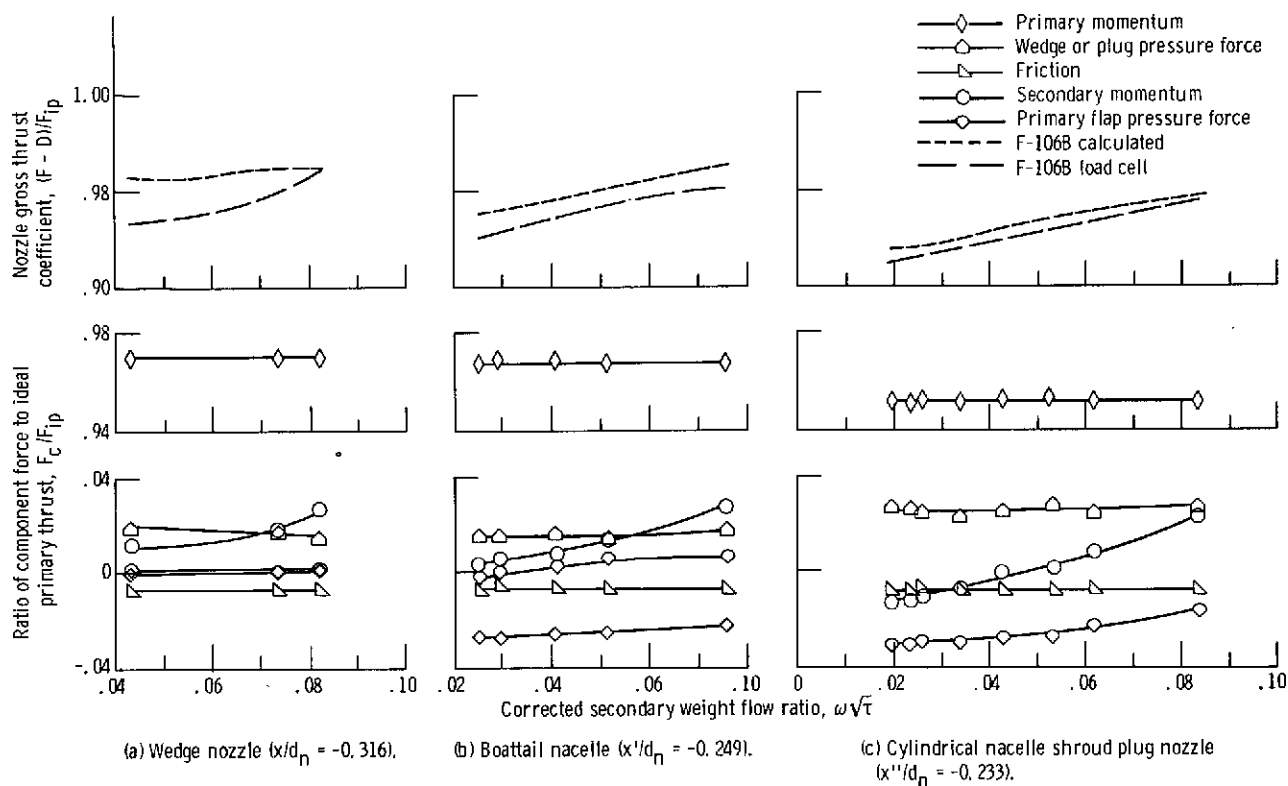


Figure 27. - Effect of secondary flow on component forces. Flight Mach 0.9; military power.